THE JOURNAL OF BIOLOGICAL CHEMISTRY VOL. 286, NO. 27, pp. 23900–23910, July 8, 2011

Crystal Structures of *Staphylococcus epidermidis* Mevalonate Diphosphate Decarboxylase Bound to Inhibitory Analogs Reveal New Insight into Substrate Binding and Catalysis*[S]

Received for publication, March 21, 2011, and in revised form, April 26, 2011 Published, JBC Papers in Press, May 11, 2011, DOI 10.1074/jbc.M111.242016

Michael L. Barta[‡1], D. Andrew Skaff[§1], William J. McWhorter[‡], Timothy J. Herdendorf[§], Henry M. Miziorko[§2,3], and Brian V. Geisbrecht[‡2,4]

From the Divisions of [‡]Cell Biology and Biophysics and [§]Molecular Biology and Biochemistry, School of Biological Sciences, University of Missouri-Kansas City, Kansas City, Missouri 64110

The polyisoprenoid compound undecaprenyl phosphate is required for biosynthesis of cell wall peptidoglycans in Gram-positive bacteria, including pathogenic *Enterococcus*, *Streptococcus*, and *Staphylococcus* spp. In these organisms, the mevalonate pathway is used to produce the precursor isoprenoid, isopentenyl 5-diphosphate. Mevalonate diphosphate decarboxylase (MDD) catalyzes formation of isopentenyl 5-diphosphate in an ATP-dependent irreversible reaction and is therefore an attractive target for inhibitor development that could lead to new antimicrobial agents. To facilitate exploration of this possibility, we report the crystal structure of *Staphylococcus epidermidis* MDD (1.85 Å resolution) and, to the best of our knowledge, the first structures of liganded MDD. These structures include MDD bound to the mevalonate 5-diphosphate analogs diphosphoglycolyl proline (2.05 Å resolution) and 6-fluoromevalonate diphosphate (FMVAPP; 2.2 Å resolution). Comparison of these structures provides a physical basis for the significant differences in K_i values observed for these inhibitors. Inspection of enzyme/inhibitor structures identified the side chain of invariant Ser^{192} as making potential contributions to catalysis. Significantly, Ser → Ala substitution of this side chain decreases k_{cat} by ~10^3-fold, even though binding interactions between FMVAPP and this mutant are similar to those observed with wild type MDD, as judged by the 2.1 Å cocrystal structure of S192A with FMVAPP. Comparison of microbial MDD structures with those of mammalian counterparts reveals potential targets at the active site periphery that may be exploited to selectively target the microbial enzymes. These studies provide a structural basis for previous observations regarding the MDD mechanism and inform future work toward rational inhibitor design.

The ever-growing trend among many bacterial pathogens toward antibiotic resistance represents one of the single greatest threats to public health in both developing and modern nations. In particular, a growing body of literature from the last decade has demonstrated that many strains of the widespread Gram-positive organisms *Staphylococcus aureus* and *Staphylococcus epidermidis* are now insensitive toward an array of the β-lactam class antibiotics that were once considered frontline therapeutics (1, 2). As recently as a few years ago, the problem of antibiotic resistance was associated primarily with those infections arising from within the healthcare setting. However, recent studies have shown that resistant strains are now spreading rapidly within the community, where they may cause potentially life-threatening illness in persons not recently hospitalized or undergoing invasive medical procedures (1, 3). Given the limited nature of effective therapeutic tools to combat these diseases, all such infections must be carefully managed to prevent further spread throughout the population. As a consequence, there is now renewed interest in novel classes of antimicrobials that are effective against sensitive and resistant strains alike.

In all eubacteria, the C_{55} polyisoprenoid molecule undecaprenyl phosphate is an essential intermediate in the biosynthesis of the peptidoglycan polymer that comprises an integral component of the cell wall. As a polyisoprenoid, undecaprenyl phosphate is synthesized in stepwise fashion from the building block isopentenyl 5-diphosphate (IPP).[5] Whereas IPP is generated via the methylerythritol phosphate pathway in Gram-negative organisms (4), many Gram-positive pathogens (including those mentioned above) rely on the mevalonate pathway for its synthesis (5). The mevalonate pathway produces one molecule of IPP from three molecules of acetyl-CoA in six enzymatic steps. Of these, five have been shown to be essential for the

* This work was supported in part by National Institutes of Health Grants AI071028 and AI090149.

[S] The on-line version of this article (available at http://www.jbc.org) contains supplemental Figs. S1 and S2 and Tables S1 and S2.

The atomic coordinates and structure factors (codes 3QT5, 3QT6, 3QT7, and 3QT8) have been deposited in the Protein Data Bank, Research Collaboratory for Structural Bioinformatics, Rutgers University, New Brunswick, NJ (http://www.rcsb.org/).

[1] Both authors contributed equally to this work.

[2] Both authors shared supervision of this work.

[3] To whom correspondence may be addressed: School of Biological Sciences, University of Missouri-Kansas City, 5100 Rockhill Rd., Kansas City, MO 64110. Tel.: 816-235-2246; Fax: 816-235-5595; E-mail: MiziorkoH@umkc.edu.

[4] To whom correspondence may be addressed: School of Biological Sciences, University of Missouri-Kansas City, 5100 Rockhill Rd., Kansas City, MO 64110. Tel.: 816-235-2592; Fax: 816-235-1503; E-mail: GeisbrechtB@umkc.edu.

[5] The abbreviations used are: IPP, isopentenyl diphosphate; MDD, mevalonate diphosphate decarboxylase; DPGP, diphosphoglycolyl proline; MVAPP, mevalonate 5-diphosphate; FMVAPP, 6-fluoromevalonate 5-diphosphate; GHMP, galactokinase, homoserine kinase, mevalonate kinase, phosphomevalonate kinase; ATPγS, adenosine 5′-*O*-(thiotriphosphate); AMP-PCP, adenosine 5′-(β,γ-methylenetriphosphate); PDB, Protein Data Bank.

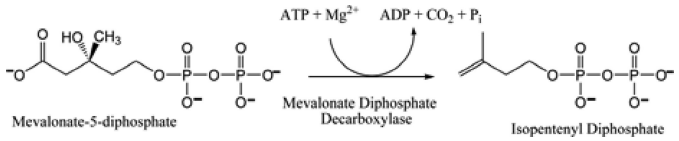

REACTION 1

growth of various Gram-positive organisms (5), presumably because of their requirement for providing IPP groups needed for synthesis of menaquinone (for ATP production) as well as undecaprenyl phosphate (for peptidoglycan production). Because compounds that selectively inhibit any of the enzymatic reactions required for bacterial cell wall biogenesis have been recognized for their potential value as antimicrobial agents, the enzymes of the mevalonate pathway present new, attractive targets for the identification and development of next-generation antibiotics. Importantly, these targets have not yet been exploited for such purposes, making it very likely that potential drug candidates will have activity against resistant strains of Gram-positive pathogens.

The enzyme mevalonate diphosphate decarboxylase (MDD; EC 4.1.1.33) catalyzes the final step of the mevalonate pathway, where it produces IPP from mevalonate 5-diphosphate (MVAPP) in an irreversible reaction dependent upon Mg^{2+}-ATP. The reaction proceeds as shown in Reaction 1. As the mevalonate pathway is present in fungi, protists, and higher eukaryotes, the MDD reaction is well established, and MDD enzymes have been extensively characterized from yeast (6, 7), avian (8), and mammalian sources (9–11). Together, these results have elucidated many details of the MDD mechanism.[6] In particular, the side chain of Asp^{283} has been assigned the role of a general base, which serves to deprotonate the MVAPP C3 alcohol and to promote formation of a metastable 3-phospho-MVAPP adduct. Departure of this phosphoryl leaving group allows a carbocation intermediate to develop at C3. It is this, in conjunction with interactions between the C1 carboxylate and the guanidinium group Arg^{144}, that drives subsequent decarboxylation and production of IPP. Indeed, mutation of either of these side chains results in a 3–5 order of magnitude decrease in catalysis (7, 11).

MDD proteins are members of the galactokinase, homoserine kinase, mevalonate kinase, and phosphomevalonate kinase (GHMP kinase) family (12). These enzymes are characterized by a cone-shaped fold, where the β-grasp-like N-terminal region packs orthogonally against the relatively planar C-terminal region comprised of five prominent α-helices (13). High resolution crystal structures of MDD proteins have been reported from a number of species across several kingdoms of life, including *S. aureus* (13), *Trypanosoma brucei* (13), *Saccharomyces cerevisiae* (12), as well as *Homo sapiens* (11). These structures reveal the presence of a deep cleft that forms between the roughly equal halves of the enzyme, which houses the catalytic Asp and Arg residues. Despite the importance of this work, a significant limitation of all MDD structures published to date is the absence of any bound ligands at the active site. Consequently, a detailed and direct identification of substrate-binding residues has remained elusive.

To clarify previous observations regarding the MDD mechanism and to better understand the basis for substrate recognition by MDD proteins, we report here the high resolution x-ray crystal structures of *S. epidermidis* MDD both free and bound to the inhibitory substrate analogs diphosphoglycolyl proline (DPGP) and 6-fluoromevalonate diphosphate (FMVAPP). In addition to providing a physical basis for differences in inhibitory potency between these two molecules, this work has identified a new residue, Ser^{192}, that contributes to catalysis by MDD. Furthermore, a significant sequence/structure difference between bacterial and eukaryotic MDDs at position 193 has also been identified. These studies inform structure/function relationships and highlight subtle yet noteworthy differences within diverse MDD proteins. The results will inform future work on developing selective MDD inhibitors that may be evaluated for their antimicrobial properties.

EXPERIMENTAL PROCEDURES

Cloning, Overexpression, and Purification of Recombinant Forms of MDD—A gene fragment encoding the entire open reading frame (residues 1–327) of MDD was amplified from *S. epidermidis* genomic DNA via PCR and subcloned into the expression plasmid pT7HMT (14). Upon confirmation of its DNA sequence, this plasmid was transformed into BL21 (DE3) *Escherichia coli* cells, and the resulting strain was cultured in Terrific Broth supplemented with kanamycin (50 μg/ml) at 37 °C to an $A_{600\ nm}$ of 0.8. Protein expression was induced overnight at 18 °C by adding isopropyl 1-thio-β-D-galactopyranoside to a 1 mM final concentration. Bacterial cells were harvested by centrifugation, resuspended in lysis buffer (20 mM Tris-HCl (pH 8.0), 500 mM NaCl, and 10 mM imidazole), and then lysed by microfluidization. The soluble tagged protein was collected in the supernatant following centrifugation of the cell homogenate and purified on a Ni^{2+}-NTA-Sepharose column according to published protocols (14). Recombinant tobacco etch virus (TEV) protease was used to digest the fusion affinity tag from the target protein; however, following removal of the affinity tag, the sequence GSTGS remains at the enzyme N terminus as an artifact of the subcloning procedure. After desalting into 20 mM Tris-HCl (pH 8.0), final purification was achieved by ResourceQ anion-exchange chromatography (GE Healthcare). Following this, the purified protein was concentrated to 5 mg/ml and buffer exchanged by ultrafiltration into 10 mM Tris-HCl (pH 7.5), 50 mM NaCl, and stored at 4 °C for further use. An analogous expression vector for the S192A mutant was constructed using standard molecular biology techniques (15). The mutant enzyme was purified and stored in an identical manner to the wild type protein.

Substrates and Analogs—The synthesis of MVAPP has been previously reported (16) and is briefly summarized. Methyl 3-hydroxy-3-methyl-5-iodopentanoate was synthesized by reacting mevalonolactone with trimethylsilyl iodide, followed by diazomethane derivatization to form the methyl ester. The product was subsequently purified by silica gel chromatography. Methyl 5-diphosphomevalonate was synthesized by reacting the purified methyl 3-hydroxy-3-methyl-5-iodopentanoate with an

[6] Numbering of all residues in this work reflects their position in the *S. epidermidis* MDD sequence.

excess of tetrabutylammonium diphosphate. This material was purified using a DEAE-Sephadex A-25 (bicarbonate form) column. The purified methyl 5-diphosphomevalonate was converted to the lithium salt using Dowex 50 (lithium form). Deesterification was accomplished by alkaline hydrolysis in 0.5 N LiOH for 20 h at 4 °C. The pH was adjusted to ~8.0 with cold HCl, and the concentration of the physiologically active *R* isomer was determined using MDD for an enzymatic end point assay.

Preparation of FMVAPP employed the method described by Voynova *et al.* (11). Five milligrams (33.8 μmol) of (*RS*)-6-fluoromevalonolactone was delactonized in 0.1 N KOH by incubation for 1 h at 37 °C prior to neutralization. The reaction mixture for the formation of FMVAPP included the following in 1.5 ml: 30 mM Tris-HCl (pH 7.5), 22.5 mM (*RS*)-6-fluoromevalonate, 5 mM ATP, 6 mM $MgCl_2$, 0.7 mM DTT, 50 mM phosphoenolpyruvate, 6 units of pyruvate kinase, and 2.7 units of mevalonate kinase. The reaction was incubated at 30 °C. 16.9 μmol of (*R*)-6-fluoromevalonate were converted to the monophosphate in 1 h as determined by a phosphomevalonate kinase end point assay. Phosphomevalonate kinase (4 units of human enzyme) was then added, and the incubation was continued at 25 °C for 12 h. 10 μmol (~60%) of the (*R*)-6-fluoromevalonate 5-phosphate was converted to the diphosphate as determined with phosphomevalonate kinase (reverse reaction). The reaction mixture was deproteinized (95 °C for 3 min), cooled to 0 °C, and centrifuged for 15 min at 16,100 × *g*, and the supernatant was adjusted to pH ~5.0. Nucleotides were precipitated with cold ethanol (65% v/v for 30 min). Ethanol was removed from the supernatant by evaporation, and the sample was adjusted to pH ~8.0 prior to dilution and chromatographic purification (DEAE Sephadex A-25).

The competitive inhibitor DPGP was synthesized by the strategy of Vlattas *et al.* (18). Detailed methodology has been described by Krepkiy and Miziorko (19).

Kinetic Characterization of Wild Type and Mutant S. epidermidis MDD—Enzymatic activity was determined using a spectrophotometric assay coupling product ADP formation to pyruvate kinase/lactate dehydrogenase oxidation of NADH at 340 nm using a PerkinElmer Life Sciences 35 spectrophotometer. Assays were performed at 30 °C in 100 mM HEPES-NaOH (pH 7.0) containing 100 mM KCl, 10 mM $MgCl_2$, 0.2 mM NADH, 0.4 mM phosphoenolpyruvate, and 4 units each of pyruvate kinase and lactate dehydrogenase. All assays were initiated by addition of MVAPP. V_{max} and K_m values (Table 1) were determined by fitting data to the Michaelis-Menten equation. For inhibition kinetics, substrate (MVAPP) was varied *versus* inhibitor concentrations for FMVAPP or DPGP. Optimal data fits (R^2 >0.97) were obtained using either competitive (FMVAPP) or mixed (DPGP) inhibition models. All kinetic data analysis was performed using SigmaPlot 10.0/Enzyme Kinetics Module 1.3 (Systat Software, Inc.). FMVAPP concentrations varied from 40 to 320 nM. DPGP concentrations varied from 3 to 10 μM.

Crystallization—Recombinant *S. epidermidis* MDD was crystallized by vapor diffusion of hanging drops at 20 °C. Specifically, 1 μl of protein solution (5 mg/ml in 10 mM Tris-HCl (pH 7.5), 50 mM NaCl) was mixed with 1 μl of reservoir solution containing 0.25 M sodium formate and 16% (w/v) PEG 3350 that had been previously diluted in an equal volume of double distilled H_2O and equilibrated over 500 μl of reservoir solution. Single block-shaped crystals appeared after 2 days and continued to grow in size for ~3 days. Crystals were flash-cooled in a cryoprotectant solution consisting of reservoir buffer with an additional 15% (v/v) glycerol. Cocrystallization of MDD with a molar excess (~0.5 mM) of both DPGP and FMVAPP was achieved in the same manner as described above. Cocrystals of the S192A mutant MDD bound to FMVAPP were obtained in the same manner as for wild type MDD.

Diffraction Data Collection, Structure Determination, Refinement, and Analysis—Monochromatic x-ray diffraction data were collected from single crystals at 100 K using beamline 22-BM of the Advanced Photon Source, Argonne National Laboratory (Table 2). Following data collection, individual reflections were indexed, integrated, merged, and scaled using HKL2000 (20). Initial phase information was obtained for the unbound MDD structure by maximum-likelihood molecular replacement using PHASER (21). Specifically, chain A of PDB entry 2HK2 (*S. aureus* MDD) was altered using the SWISS-MODEL server to reflect the sequence of *S. epidermidis* MDD (22, 23), and the resulting hypothetical structure was used as a search model. The single most highly scored solution contained an MDD dimer in the asymmetric unit; this arrangement corresponded to a Matthews coefficient of 2.23 $Å^3$/Da and a solvent content of 45.0%. The refined structure of unliganded MDD (as obtained below) was used as a search model for all other structures reported here.

Structure refinement was carried out using phenix.refine (24). One round of simulated annealing, individual coordinates, and isotropic atomic displacement factor refinement were conducted, and the refined model was used to calculate both $2F_o - F_c$ and $F_o - F_c$ difference maps. These maps were used to iteratively improve the model by manual building in Coot (25, 26), followed by additional coordinate and atom displacement factor refinement. A final cycle of TLS refinement was also used to complete the structure of wild type MDD bound to FMVAPP. Ordered solvent molecules were added to all structures according to the default criteria of phenix.refine and inspected manually using Coot prior to model completion. Additional information and refinement statistics for all four structures are presented in Table 2.

With the lone exception of chain A in the DPGP-bound structure, a region of poor map quality exists between residues 184 and 194 in all MDD structures reported here. The exact number of residues that could not be modeled ranged between two and six, varying among the chains and structures. Further details regarding the residues that could not be modeled accurately may be found in the corresponding PDB files.

Ligand Fitting—Models for each ligand were generated using the PRODRG server (27), and restraint files were generated using phenix.elbow (24). In all cases reported here, inspection of the initial $F_o - F_c$ maps described above revealed unmodeled contiguous density that corresponded to ordered ligand in the active site of both copies of MDD found within the asymmetric unit. phenix.ligandfit (24) was subsequently used to fit and model an inhibitor molecule in each active site. Refinement of inhibitor-bound MDD structures was carried out as described above, with the exception that constrained group occupancy

TABLE 1
Comparison of kinetic parameters for MDD from *S. epidermidis* and other sources

Parameter[a]	*S. epidermidis* MDD	*S. epidermidis* S192A	*S. aureus* MDD	*T. brucei* MDD	*H. sapiens* MDD[b]	*Gallus gallus* MDD[c]
V_{max} (units/mg)	9.8 ± 0.3	0.0096 ± 0.0003	9.8 ± 0.2	8.8 ± 0.2	6.1 ± 0.5	6.3
k_{cat} (s^{-1})	5.9 ± 0.2	0.0058 ± 0.0002	6.0 ± 0.1	6.1 ± 0.1	4.4 ± 0.4	4.5
$K_{m((RS)\text{-MVAPP})}$ (μM)	9.1 ± 0.9	5.0 ± 1.0	22.3 ± 1.6	6.0 ± 0.4	28.9 ± 3.3	14.1
$K_{m(\text{ATP})}$ (mM)	0.027 ± 0.003	0.07 ± 0.01	0.013 ± 0.001	0.30 ± 0.02	0.69 ± 0.07	0.50
$K_{i((R)\text{-FMVAPP})}$ (nM)	49 ± 5	ND	ND	22.8 ± 3.8	62 ± 5	ND
$K_{i((RS)\text{-DPGP})}$ (μM)	4.3 ± 1.0[d]	ND	ND	ND	2.3 ± 0.3	ND

[a] ND indicates value has not been determined.
[b] Estimates were reported by Voynova *et al.* (11).
[c] Estimates were reported by Alvear *et al.* (8).
[d] $K_{i\ \text{slope}}$ value is reported. Mixed (noncompetitive) inhibition was observed.

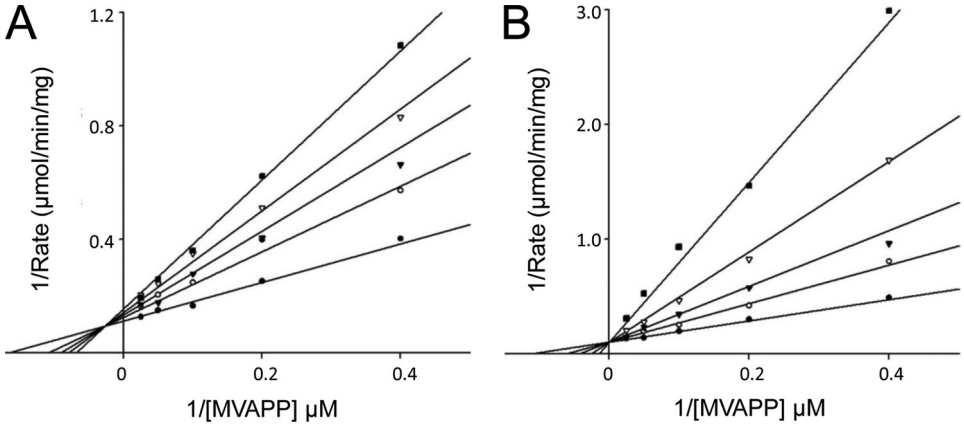

FIGURE 1. **Inhibition of *S. epidermidis* MDD by MVAPP analogs.** Double-reciprocal plots of MDD activity *versus* substrate MVAPP concentration are shown as measured in the presence of either DPGP or FMVAPP. *A*, inhibition of MDD by DPGP. Concentrations of DPGP are as follows: 0 μM (●), 3 μM (○), 5 μM (▼), 7 μM (▽), and 10 μM (■). *B*, inhibition of MDD by FMVAPP. Concentrations of FMVAPP are as follows: 0 nM (●), 40 nM (○), 80 nM (▼), 160 nM (▽), and 320 nM (■). Concentrations of substrate (MVAPP) were 2.5, 5, 10, 20, and 40 μM in both panels. Optimal fits to the data were obtained using a mixed inhibition model in *A* and a competitive inhibition model in *B*.

refinement was used to estimate the fraction of ligand bound at each site independently.

Miscellaneous—Multiple sequence alignments were carried out using ClustalW (28) and aligned with secondary structure elements using ESPRIPT (29). MDD sequences used in alignments, along with their respective GenBank™ accession numbers, were as follows: *S. epidermidis*, 27467280; *S. aureus*, 14246359; *Legionella pneumophila* subsp. *pneumophila*, 52842257; *Streptococcus pyogenes*, 5093120; *H. sapiens*, 4505289; *S. cerevisiae*, 1706682; *T. brucei*, 149241992; *Mus musculus*, 13539580; *Listeria monocytogenes*, 217965923; *Enterococcus faecalis*, 315577315; *Xenopus* (*Silurana*) *tropicalis*, 39645379; *Bos taurus*, 115495513; *Arabidopsis thaliana*, 18410026. Three-dimensional structures were superimposed using the Local-Global Alignment method (LGA) (30). MDD structures were obtained from the PDB (31) and are as follows: *S. cerevisiae* (1FI4); *S. pyogenes* (2GS8); *S. aureus* (2HK2 and 2HK3); *T. brucei* (2HKE); *H. sapiens* (3DJ4); *M. musculus* (3F0N); *L. pneumophila* (3LTO). Representations of all structures were generated using PyMol (32). Calculations of electrostatic potentials at the molecular surface were carried out using DELPHI (33, 34). The program CONSURF was used to plot levels of amino acid sequence conservation on the molecular surface (35).

RESULTS

Kinetic Characterization and Crystal Structure of MDD from S. epidermidis—Whereas MDD proteins have been previously described from a variety of organisms, the nature of this enzyme in the pathogen *S. epidermidis* has so far been undetermined. To this end, a BLAST search was conducted using *S. aureus* MDD as a query sequence (36), which identified an as yet uncharacterized protein that shared 73% identity across the entire 327-residue polypeptide. A cDNA corresponding to this open reading frame was amplified by *S. epidermidis* genomic DNA by PCR and subcloned into an expression vector, and the resulting protein was expressed recombinantly and isolated from *E. coli*. The purified protein was characterized using the assay described under "Experimental Procedures." The results of this analysis demonstrated that this *S. epidermidis* protein is a *bona fide* MDD that exhibits kinetic constants of V_{max} = 9.8 units/mg, $K_{m,(RS)\text{-MVAPP}}$ = 9.1 μM, and $K_{m(\text{ATP})}$ = 27 μM (Table 1). These values are comparable to corresponding parameters reported for most other MDD enzymes, although the prokaryotic MDD enzymes exhibit lower K_m values for ATP than reported for eukaryotic enzymes. In all cases, $K_{i(\text{FMVAPP})}$ (<100 nM) indicates high affinity binding, whereas the analog DPGP inhibits 40–90-fold more weakly to human and *S. epidermidis* MDD, respectively (Fig. 1 and Table 1). Table 1 also includes kinetic parameter data for previously uncharacterized *S. aureus* and *T. brucei* MDD proteins (for which unliganded structures have been determined (13)), demonstrating that these proteins efficiently catalyze the MDD reaction.

To better understand the nature of this enzyme, purified *S. epidermidis* was entered into crystallization trials using a hanging drop vapor diffusion approach. Following optimization of initial crystals, the final samples diffracted synchrotron x-rays

TABLE 2
Diffraction data collection and structure refinement statistics

Data collection[a]				
Crystal	MDD	MDD + DPGP	MDD + FMVAPP	S192A + FMVAPP
Beamline	APS 22-BM	APS 22-BM	APS 22-BM	APS 22-BM
Wavelength	1.000 Å	1.000 Å	0.9724 Å	1.000 Å
Space group	$C222_1$	$C222_1$	$C222_1$	$C222_1$
Cell dimensions	$a = 82.98$ $b = 101.99$ $c = 155.77$	$a = 82.67$ $b = 101.44$ $c = 154.64$	$a = 82.80$ $b = 101.49$ $c = 155.56$	$a = 82.50$ $b = 101.37$ $c = 155.26$
Resolution	26.91-1.85 Å	29.60-2.05 Å	30.70-2.20 Å	29.00-2.10 Å
Reflections (unique)	307, 824 (52,638)	573,361 (41,249)	486,156 (33,608)	211,067 (34,043)
Completeness	92.7% (81.5%)	100.0% (100.0%)	100.0% (99.9%)	88.8% (87.5%)
Redundancy	5.8-Fold	13.9-Fold	14.5-Fold	6.2-Fold
$\langle I\rangle/\langle\sigma I\rangle$	25.2 (2.5)	26.6 (5.1)	20.0 (5.0)	19.5 (2.9)
R_{merge}[b]	5.8% (60.3%)	9.1% (50.5%)	10.9% (46.0%)	7.9% (53.2%)
Refinement				
PDB code	3QT5	3QT6	3QT7	3QT8
Protein molecules/asymmetric unit	2	2	2	2
R_{work}/R_{free}[c]	19.5/22.7%	18.3/22.6%	17.8/22.5%	19.0/24.1%
No. of atoms				
Protein	5078	5078	5038	5065
Ligand	NA[d]	40	38	38
Solvent	389	312	243	284
Ramachandran plot				
Favored	98.1%	98.1%	98.1%	98.4%
Allowed	1.7%	1.6%	1.4%	1.6%
Outliers	0.2%	0.3%	0.5%	0%
Root mean square deviation				
Bond length	0.007 Å	0.008 Å	0.007 Å	0.008 Å
Bond angle	0.99°	1.03°	1.07°	1.09°
B factor				
Protein	27.1 Å^2	31.2 Å^2	33.0 Å^2	32.0 Å^2
Ligand	NA	30.0 Å^2	25.1 Å^2	26.2 Å^2
Solvent	30.2 Å^2	33.5 Å^2	33 Å^2	32.0 Å^2
Ligand occupancy				
Chain A	NA	80%	100%	100%
Chain B	NA	92%	100%	100%

[a] Numbers in parentheses are for the highest resolution shell.
[b] $R_{merge} = \Sigma_h\Sigma_i|I_i(h) - \langle I(h)\rangle|/\Sigma_h\Sigma_i I_i(h)$, where I_i (h) is the ith measurement of reflection h, and $\langle I(h)\rangle$ is a weighted mean of all measurements of h.
[c] $R = \Sigma_h|F_{obs}(h) - F_{calc}(h)|/\Sigma_h|F_{obs}|$. R_{cryst} and R_{free} were calculated from the working and test reflection sets, respectively. The test set constituted 5% of the total reflections not used in refinement.
[d] NA means not applicable.

to 1.85 Å resolution (Table 2). The *S. epidermidis* MDD structure was solved by molecular replacement and subsequently refined to final R_{work} and R_{free} values of 19.5 and 22.7%, respectively (Fig. 2*A*). This structure adopts a canonical GHMP kinase fold and displays a high degree of homology to those of related MDD proteins (Fig. 2*B*), even though these enzymes collectively share a rather limited sequence identity with one another. For example, *S. epidermidis* MDD is only 34% identical with the human enzyme, yet 300 of its 327 backbone atoms superimpose at less than 4.0 Å distance of their corresponding positions with a root mean square deviation of 1.54 Å (30).

S. epidermidis MDD behaves as a dimer of 36-kDa subunits in analytical gel filtration chromatography experiments (supplemental Fig. S2). Consistent with this, the MDD polypeptide is found as a dimer within the asymmetric unit of its centered orthorhombic crystal. This quaternary structure buries 1950 Å^2 or nearly 7% of the available surface area when both protein chains are considered together. This is comparable to the observation of a dimer interface of 7.7% (2250 Å^2) for rat mevalonate kinase (37), which also exhibits the GHMP kinase fold. Although examination of neighboring asymmetric units reveals the presence of alternative modes for dimerization, only this interface is predicted to be significantly thermodynamically favored in solution, as judged by the protein interface surfaces and assemblies (PISA) server (38). These considerations aside, the entrance to the active site cavity is unhindered by any of the potential dimerization contacts described here. Thus, although observation of a dimeric species for MDD is typical, it is unclear that a dimeric enzyme is required for catalysis.

Structural Basis for Substrate Recognition and Competitive Inhibition of MDD—Prior crystallographic studies on MDD proteins have been limited to the unliganded form of the enzyme, which has precluded detailed analysis of both their structure/function relationships and modes of substrate binding. In two cases in particular (*i.e. S. aureus* and *T. brucei* (13)), attempts to obtain an informative ligand-bound structure were unsuccessful, presumably because of the presence of well ordered sulfate ions found within the purported active site cleft of these enzymes (13). Examination of additional MDD structures available in the PDB suggests that moderate to high concentrations of sulfate anions indeed promote crystallization of these enzymes, as five of the seven structures resulted from crystals harvested from sulfate-containing mother liquids. In this regard, the fact the crystals of *S. epidermidis* MDD grow readily in the absence of sulfate raised the possibility that this specific enzyme may be more amenable to determination of a structure with bound ligand.

Previous investigation into the MDD mechanism has identified two separate diphosphorylated compounds, DPGP (11) and FMVAPP (16, 39), that mimic the MVAPP substrate and competitively inhibit MDD activity (11). Despite these similarities, characterization of their effects on *S. epidermidis* MDD

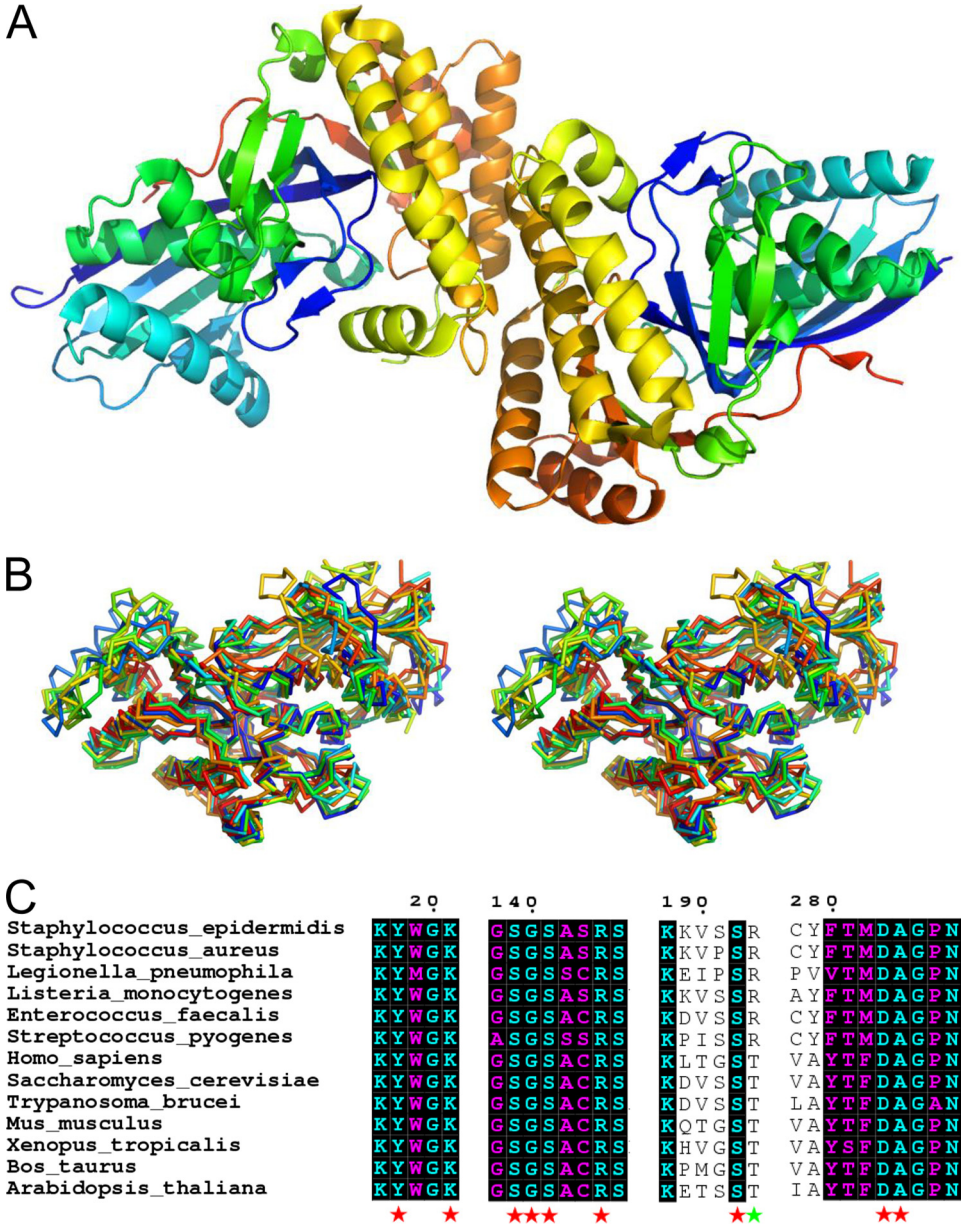

FIGURE 2. **1.85 Å crystal structure of apo-MDD from *S. epidermidis*.** *A*, crystal structure of *S. epidermidis* MDD shown in *ribbon* format. Two copies of MDD are found within the asymmetric unit and are colored *blue* (N terminus) and *red* (C terminus). *B*, stereo view of MDD structures in *ribbon* format deposited within the PDB. Structures correspond to the following organisms: *S. epidermidis* (*red-orange*); *S. aureus* (*cyan*); *L. pneumophila* (*orange*); *S. pyogenes* (*red*); *H. sapiens* (*yellow-green*); *S. cerevisiae* (*blue*); *T. brucei* (*green*); and *M. musculus* (*yellow*). *C*, limited structure-based sequence alignment of prokaryotic and eukaryotic MDD proteins. Alignment was generated using ClustalW and rendered with ESPRIPT. *Numbers above* the sequences correspond to *S. epidermidis* MDD. *Red stars below* the sequences correspond to invariant amino acid side chains involved in DPGP and FMVAPP interaction, and the *green star* represents the single variable active site residue. Sequences from *B* as well as the following were used in alignment: *L. monocytogenes*; *E. faecalis*; *Xenopus. tropicalis*; *B. taurus*; *A. thaliana*.

revealed markedly different K_i values of 4 μM for DPGP and 49 nM for FMVAPP (Table 1). A similar trend was also observed for the same inhibitors and human MDD, where the observed K_i values were 2 μM and 62 nM, respectively. Because comparison of K_i values for competitive inhibitors and $K_{i\ \mathrm{slope}}$ values for mixed inhibitors primarily reflects differences in binding affinity, these data suggested that meaningful insight into both the catalytic mechanism and mode of substrate binding by MDD proteins could be revealed by determining the cocrystal structures of *S. epidermidis* MDD bound to DPGP and FMVAPP.

Crystals of MDD grown in the presence of (*RS*)-DPGP diffracted x-rays to 2.05 Å limiting resolution (Table 2). Following modeling and refinement of two copies of MDD, analysis of an $F_o - F_c$ difference map revealed a region of strong contiguous density within the MDD active site cleft (Fig. 3*A*) (11). Placement and refinement of a single (*R*)-DPGP molecule per enzyme monomer (occupancy of 0.80 and 0.92 in chain A and B, respectively) are in good agreement with the observed diffraction data (Table 2 and Fig. 3*B*). Significantly, the conformations of both (*R*)-DPGP molecules, bound selectively from the *R,S* mixture, are nearly indistinguishable from one another, as all 24

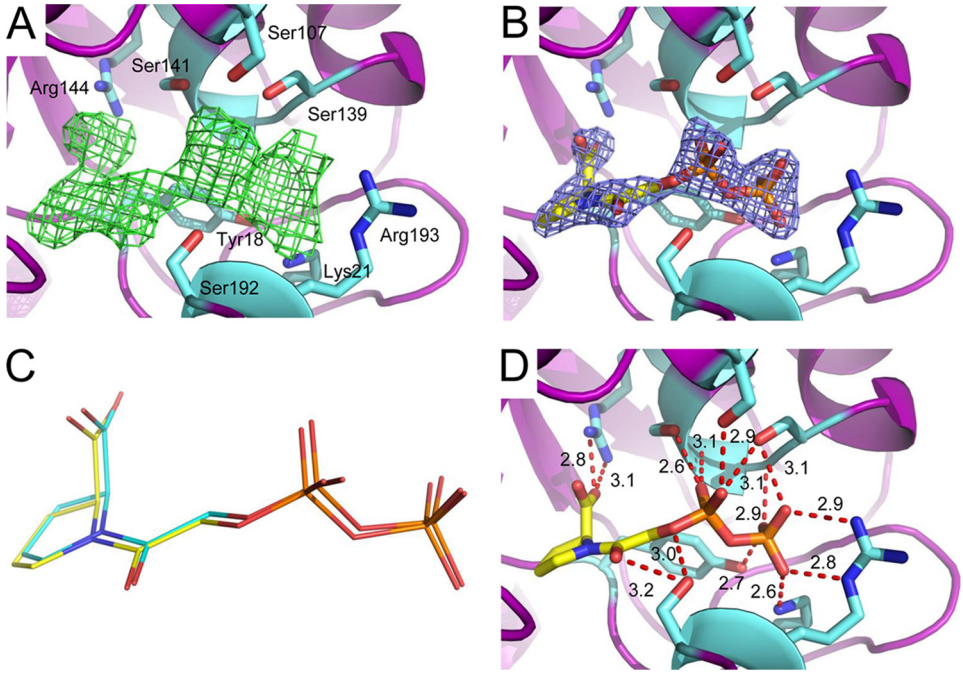

FIGURE 3. **2.05 Å cocrystal structure of MDD bound to the inhibitor DPGP.** *A*, $F_o - F_c$ map (*green mesh* at 2.0σ contour) of the refined structure in the absence of modeled ligand. Active site side chains within interaction distance are depicted in *ball and stick* format (*cyan*). MDD backbone is depicted in *ribbon* format (*purple*). *B*, $2F_o - F_c$ map (*blue mesh* at 2.0σ contour) of the refined structure with one molecule DPGP modeled per enzyme. Color scheme is the same as *A*, with DPGP colored *yellow*. *C*, overlay of DPGP molecules from the active sites of chains A (*yellow*) and B (*cyan*). *D*, active site side chains within 2.6–3.4 Å of DPGP. Further information on these distances can be found in supplemental Table S1.

atoms modeled superimpose with root mean square deviation values of 0.75 Å (Fig. 3*C*).

Numerous invariant amino acid side chain and backbone atoms contribute to the strong interaction of MDD with DPGP (Figs. 2*C* and 3*D* and supplemental Fig. S1). Several of these, including four serines (Ser^{107}, Ser^{139}, Ser^{141}, and Ser^{192}), two residues from the N-terminal most β-strand in the enzyme (Tyr^{18} and Lys^{21}), as well as Gly^{140} and Arg^{193} lie within a 3.5 Å distance of the atoms that comprise the α- and β-phosphoryl groups of DPGP. Separately, both nitrogen atoms of the catalytic Arg^{144} guanidinium group hydrogen bond with a single oxygen atom from the DPGP carboxylate (2.8 and 3.1 Å, respectively). Finally, while the available carbonyl oxygen of DPGP is also close enough to hydrogen bond with the side chain of Ser^{192} (3.2 Å), the general base Asp^{283} is notable in that it is too distant to interact with any atoms of the inhibitor.

In a similar manner, MDD crystals were grown in the presence of (*R*)-FMVAPP. These crystals diffracted x-rays to 2.20 Å limiting resolution (Table 2). Well defined electron density was likewise apparent upon inspection of the $F_o - F_c$ difference map obtained following initial refinement (Fig. 4*A*). A single copy of FMVAPP was placed in each MDD active site and refined at 100% occupancy (Table 2 and Fig. 4*B*). As was seen for DPGP, both FMVAPP molecules are bound in identical conformations, as all 19 atoms modeled superimpose with a root mean square deviation of 0.72 Å (Fig. 4*C*). Although several recurring side chain and backbone contacts from the DPGP-bound enzyme are present in the FMVAPP-inhibited structure (Figs. 2*C*, 3*D*, and 4*D* and supplemental Table S1), other unique interactions are also observed. For example, the backbone nitrogen, rather than the side chain hydroxyl, of Ser^{107} participates in a hydrogen bond with an α-phosphoryl-derived oxygen atom of FVMAPP (Fig. 4, *D* and *E*). Furthermore, several interactions that are crucial to the proposed catalytic mechanism are also seen. This includes a hydrogen bond (3.4 Å distance) between the side chain of Asp^{283} and C3 hydroxyl of FMVAPP, and each of the nitrogen atoms of the Arg^{144} guanidinium group binds to a different oxygen of the FMVAPP C1 carboxylate (2.9 and 3.1 Å). Finally, the fluoromethyl group of FMVAPP participates in an F···(H–N) hydrogen bond (3.1 Å) with the backbone amine of Ala^{284}.

Identification of Ser^{192} as New Residue That Contributes to MDD Catalysis—Earlier structure/function studies on MDD proteins have identified residues Asp^{283} (7) and Arg^{144} (11) as playing essential roles in catalysis. Furthermore, mutagenesis studies on Ser^{139} and Ser^{141} strongly suggest the influence of these residues in binding the diphosphorylated substrate MVAPP (19). Whereas these roles are readily interpreted in light of the DPGP- and FMVAPP-bound structures described above, the contributions of other residues are less certain. One such residue is Ser^{192}, which is also invariant among a large and diverse cohort of MDD proteins (supplemental Fig. S1).

Ser^{192} is positioned on the opposite side of the active site cleft from Ser^{139} and Ser^{141}, whose side chains participate directly in substrate binding. Nevertheless, Ser^{192} is also a far distance from the MVAPP atoms whose bonding patterns are altered during the MDD reaction, which suggests a role for this residue in substrate binding. Consistent with this idea, this side chain participates in hydrogen bonds with atoms from the inhibitor α-phosphoryl group in both the DPGP- and FMVAPP-bound structures. To test the role of Ser^{192} more directly, a S192A mutant of *S. epidermidis* MDD was constructed and character-

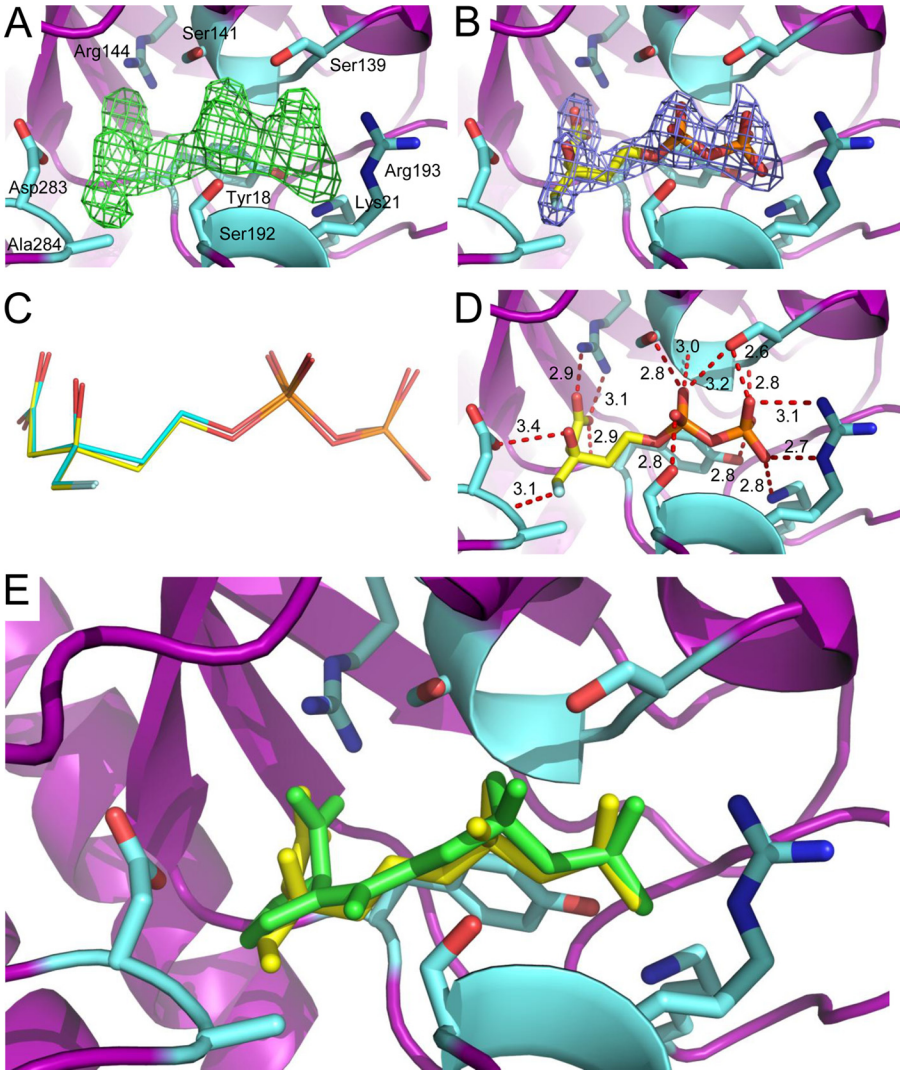

FIGURE 4. **2.20 Å cocrystal structure of MDD bound to the inhibitor FMVAPP.** *A*, $F_o - F_c$ map (*green mesh* at 3.0σ contour) of the refined structure in the absence of modeled ligand. Active site side chains within interaction distance are depicted in *ball and stick* format (*cyan*). MDD backbone is depicted in ribbon format (*purple*). *B*, $2F_o - F_c$ map (*blue mesh* at 2.0σ contour) of the refined structure with one molecule FMVAPP modeled per enzyme. Color scheme is the same as *A*, with FMVAPP colored *yellow*. *C,* overlay of FMVAPP molecules from chains A (*yellow*) and B (*cyan*). *D,* active site side chains within 2.6–3.4 Å of FMVAPP. Further information on these distances can be found in supplemental Table S2. *E,* overlay of the MDD active site from cocrystal structures of DPGP (*green*) and FMVAPP (*yellow*). Active site side chains from the FMVAPP cocrystal structure are depicted in *ball and stick* format (*cyan*).

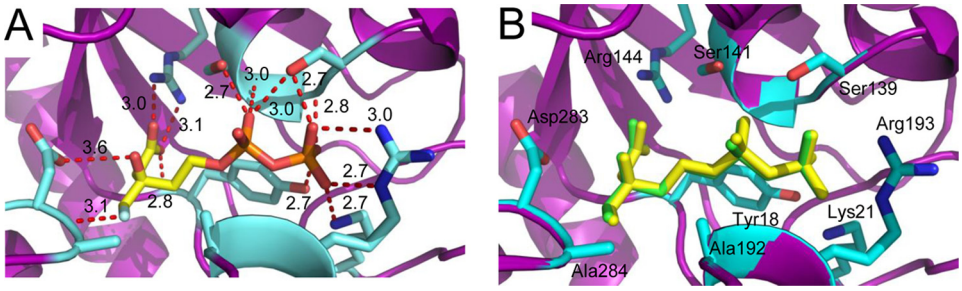

FIGURE 5. **2.10 Å cocrystal structure of MDD mutant S192A bound to the inhibitor FMVAPP.** *A*, active site side chains within 2.6–3.6Å of FMVAPP are depicted in *ball and stick* format (*cyan*). Further information on these distances can be found in supplemental Table S2. MDD backbone is depicted in *ribbon* format (*purple*). *B,* overlay of FMVAPP molecules from wild type MDD (*green*) and mutant S192A MDD (*yellow*). Color scheme is the same as *A*.

ized. Mutagenic substitutions of this side chain resulted in a near wild type K_m value for substrate binding (Table 1), a feature that agrees well with the 2.10-Å cocrystal structure of FMVAPP bound to this mutant enzyme (Fig. 5*A* and Table 2). Despite these similarities, however, the mutant exhibited a greater than thousand-fold loss of catalytic activity (k_{cat}) (Table 1). Although a detailed explanation for this effect may require a ternary ATP-FMVAPP-MDD structure, it is noteworthy that distances between the established catalytic residues (Asp^{283} and Arg^{144}) and their cognate groups on FMVAPP are greater

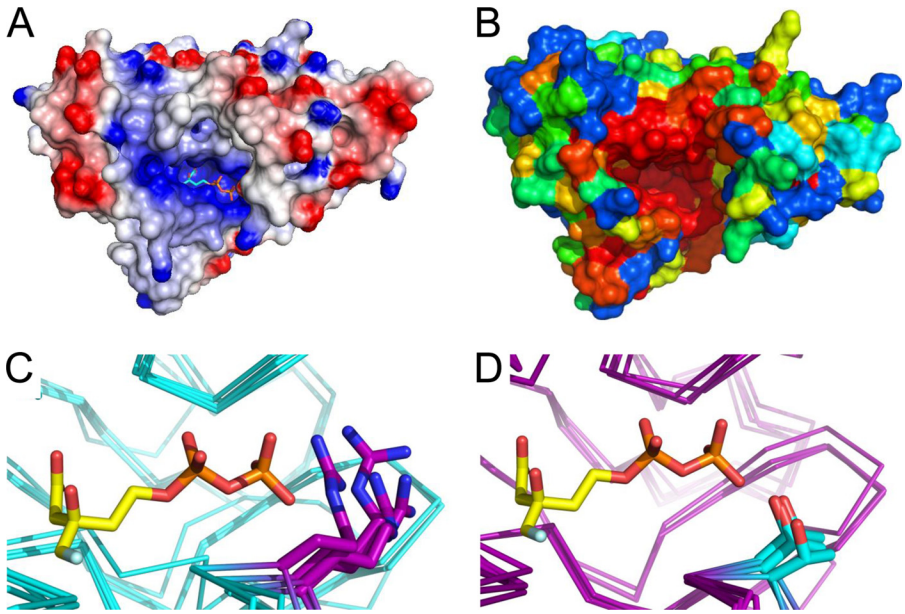

FIGURE 6. **Conserved nature of the active site cleft.** *A*, surface representation of electrostatic potential, generated by DelPhi, of chain A from MDD bound to FMVAPP (*cyan*). Color scheme represents regions of negative (*red*) and positive (*blue*) charge density contoured at ±5 *e*/*kT*. *B,* conservation plot of surface-exposed MDD amino acid side chains from *S. epidermidis,* as generated by CONSURF. Color scheme depicts variable (*blue* to *green*), average (*yellow*), and strong (*orange* to *red*) conservation. *C,* conserved nature of Arg^{193} (*purple stick*) within the active site of prokaryotic MDD proteins (backbone atoms colored *cyan*). Superimposed MDD structures are from *S. epidermidis*, *S. aureus*, *S. pyogenes*, and *L. pneumophila*. *D,* conserved nature of Thr (*cyan stick*) in eukaryotic MDD proteins (backbone atoms in *purple*) at the structurally equivalent position to Arg^{193}. Superimposed MDD structures are from *H. sapiens*, *M. musculus*, *T. brucei*, and *S. cerevisiae*. FMVAPP is shown in *C* and *D* according to its position in the wild type MDD + FMVAPP structure (Fig. 4).

in the mutant cocrystal structure when compared with wild type MDD (Fig. 5*B* and supplemental Table S2). Furthermore, the dihedral angle between the Arg^{144} guanidinium group and the FMVAPP C1 carboxylate is noticeably steeper in the mutant structure relative to that of wild type ($-29.3 \pm 1.6°$ *versus* $-18.4 \pm 2.8°$, respectively).

Conservation and Divergence in the Vicinity of the MDD Active Site Cleft—The dual substrate nature of MDD (*i.e.* MVAPP and ATP) places strict requirements on the solvent accessibility of the enzyme active site. This is magnified by the polyanionic nature of the substrates, which together carry a formal charge of −8 at physiological pH values. Consistent with these limitations, the residues lining the MDD active site entrance are overwhelmingly electropositive, and the charge density in this area is a striking feature of the MDD surface (Fig. 6*A*). The importance of this positively charged patch to substrate binding is likewise underscored by evolutionary analysis of surface-exposed MDD residues. Whereas much of the MDD surface exhibits variable levels of sequence conservation, the entrance to the active site cleft is practically invariant since the divergence of bacteria and humans (Fig. 6*B*).

The many conserved features of the MDD mechanism are highlighted by high levels of identity among residues found in the active sites of various MDD proteins. However, the ability to identify and develop highly selective competitive inhibitors requires some level of divergence between target enzymes (*i.e.* those found in bacterial cells) and those found in the human host. In this regard, examination of microbial MDD sequences and structures along with those from their protozoan, mammalian, and human counterparts reveals one obvious and significant difference within the active site (Figs. 6*C* and 2*C* and supplemental Fig. S1). Specifically, although higher order organisms have a Thr at the equivalent position to residue 193, bacterial enzymes instead harbor an Arg at this location. It is worth noting that the side chain of Arg^{193} is well ordered in all cocrystal structures determined here (*e.g.* average atomic *B* factor of 27.9 $Å^2$ relative to the mean value of 33.0 $Å^2$ for protein atoms in the MDD + FMVAPP structure), as the atoms from its guanidinium group facilitate binding to the β-phosphoryl moiety of both DPGP and FMVAPP. As a consequence, exploitation of this particular amino acid substitution may allow for future development of compounds that specifically target only bacterial MDD proteins.

DISCUSSION

MDD is a member of the large GHMP kinase family of proteins, which includes not only phosphoryl transfer enzymes but also proteins involved in development. A recent article (40) on a bacterial threonine kinase, which fits into this protein family, pointed out that family members appear to use different kinetic and catalytic mechanisms despite their common tertiary structures. These enzymes typically catalyze sequential reactions in which ATP reacts with a phosphoryl acceptor to form ADP and a phosphorylated product. Some GHMP kinases bind ATP first and acceptor substrate second (*e.g.* liver galactokinase (41) and *Salmonella enterica* threonine kinase (40)). By contrast, others bind acceptor before ATP (*e.g.* liver mevalonate kinase (42) and liver MDD (43). Yet others still appear to utilize a random order of substrate binding in proceeding to a ternary reaction complex (*E. coli* galactokinase (44) and *Streptococcus pneumoniae* phosphomevalonate kinase (45). Based upon the crystal structures presented here, it seems unlikely that MDD could function through any mechanism other than binding the MVAPP acceptor prior to ATP. This is because both the MVAPP-bind-

ing site and the catalytic residues of the enzyme lie at the bottom of the MDD active site cleft. This active site cleft resembles a funnel, rather than a shallow groove on the protein surface, so there is no conceivable route to the catalytic site that would not be greatly or completely occluded by binding to the comparatively larger nucleotide substrate. Still, a conclusive statement regarding this aspect of MDD function will require determination of a ternary complex structure. However, these observations on MDD binary complexes are in accord with the kinetic results of Jabalquinto and Cardemil (43), who productively used the dead-end competitive inhibitor method (well established by Fromm (46)) to distinguish between random, ordered, and ping-pong kinetic mechanisms for MDD. They employed mevalonate, mevalonate phosphate, ATPγS, and AMP-PCP as inhibitors and tested these against the substrates mevalonate diphosphate and ATP. The inhibition patterns that were documented unambiguously established that MDD follows a sequential kinetic mechanism in which mevalonate phosphate binds before ATP. Thus, their results represent an important test and provide independent confirmation of the structural data.

Reports suggest that different catalytic mechanisms may be used by the various GHMP kinases. For homoserine kinase, there is no structural evidence for an active site base that would enhance attack of acceptor substrate on the γ-phosphoryl of ATP, so, by default, a direct nucleophilic attack mediated by transition state stabilization has been proposed (47). For yeast galactokinase, pH dependence results were interpreted to discount any need for a catalytic base in this enzyme (48). Subsequently, these authors collaborated on a structural investigation of *Pyrococcus furiosus* galactokinase; the conclusions suggested that an active site aspartate may indeed function as a catalytic base (49). For two GHMP kinases in the mevalonate pathway, we addressed this issue by interpreting structural results in the context of functional data. In the case of rat mevalonate kinase, the binary enzyme-ATP structure indicates the proximity between Asp^{204} to the γ-phosphoryl of ATP (37). Mutagenesis results indicate that exchange of the aspartate carboxyl for either asparagine or alanine side chains that do not function as a base reduces the catalytic rate by greater than 10^4-fold. Such an effect is appropriate in magnitude for removal of a catalytic base (50). Similarly, substitution of Asp^{302} in yeast MDD with either asparagine or alanine results in $\sim 10^3$- and $\sim 10^5$-fold decreases in catalysis, respectively. Consistent with these previous observations, the results reported here indicate that the corresponding Asp^{283} is situated only 3.4 Å from the C3 hydroxyl oxygen of FMVAPP. Thus, a functional assignment of Asp^{283} as a catalytic base can now be justified on the basis of both structural proximity and mutagenesis results. When considered together, the body of literature on both mevalonate kinase and MDD strongly suggests that GHMP kinases include a subclass of enzymes that do indeed utilize an active site base to deprotonate the phosphoryl acceptor.

Perhaps there may be a reasonable alternative explanation for the role of active site aspartates in mevalonate kinase, MDD, and other GHMP kinase enzymes whose future characterization may add to this mechanistic class. This hypothesis would involve a role for aspartate in precisely positioning the substrate so that the acceptor oxygen (*i.e.* C5 oxygen in mevalonate; C3 oxygen in mevalonate diphosphate) is optimally aligned for efficient in-line phosphoryl transfer of the ATP γ-phosphoryl group. Such an explanation (17) has been proposed to account for the large diminution in catalysis (4,000-fold) that results for mevalonate kinase upon alanine substitution of Ser^{146} which, by hydrogen bonding, optimizes orientation of the phosphoryl chain of ATP (37). It is therefore likely that more structural data on GHMP kinase ternary complexes will allow a consensus to develop regarding whether general base catalysis is operative or whether substrate alignment accounts for observations such as those documented for binary complexes of mevalonate kinase and MDD. As such data develop for MDD, a more complete understanding of binding differences of DPGP or FMVAPP to MDD should become possible, although the difference in how the carboxyl groups of these analogs interact with Arg^{144} already seems clear. That being said, previous functional characterization of mutations at serines comparable to Ser^{139} and Ser^{141} was not unambiguous, as these data indicated effects on both phosphoryl acceptor and donor binding sites (19). In this regard, Ser^{107} appears to interact with phosphoryl acceptors in the binary complexes, albeit in slightly different ways, even though precedent strongly suggests that this residue is situated in a consensus binding motif for the ATP phosphoryl donor. Here again, information obtained from a ternary complex structure is likely to refine our understanding of these MDD-binding site determinants.

Because several related taxa of important human pathogens rely on the mevalonate pathway to provide the isoprenoid building blocks necessary for ATP biosynthesis and for synthesis and maintenance of the bacterial cell wall, the potential for antibiotic discovery within this pathway remains both justified and intriguing. In this regard, the absolute requirement of MDD for a functional mevalonate pathway renders this enzyme an attractive target for such work. Because crystallographic data can play a significant part in guiding inhibitor design, the crystals and structures presented here constitute a promising starting point for several reasons. First, the *S. epidermidis* MDD crystals provide the opportunity to study an enzyme from the biologically relevant situation (*i.e.* a Gram-positive pathogen) at relatively high resolution. Second, unlike the crystals described for closely related proteins (*e.g. S. aureus* MDD), the *S. epidermidis* MDD crystals grow in a condition that is free of both high concentrations of sulfate and phosphate anions. This serendipitous discovery prevents undesirable, adventitious binding of such anions in a region of the active site that contributes important determinants for recognizing the diphosphorylated substrate MVAPP. Along similar lines, the modest ionic strength of the precipitant solution (0.25 M sodium formate) appears to be amenable to cocrystallization or ligand soaking of large numbers of potential small molecule inhibitors. In this respect, determination of cocrystal structures with both DPGP and FMVAPP, two molecules whose relative affinities for the enzyme differ considerably, provides a valuable proof of principle moving forward. Finally, this approach has already uncovered a significant difference between bacterial and eukaryotic MDD active sites that may be important to designing selective inhibitors. While this work is still ongoing, it represents an

exciting basis from which future structure-activity relationship studies on small molecule inhibitors can be launched.

Acknowledgments—We acknowledge the generous technical assistance of Drs. Rod Salazar and Andy Howard during x-ray diffraction data collection and Dr. Samuel Bouyain for comments on the manuscript. Drs. Imogen Wilding and William Hunter generously provided plasmids used for production and characterization of S. aureus MDD and T. brucei MDD, respectively. Use of the Advanced Photon Source was supported by the United States Department of Energy, Office of Science, Office of Basic Energy Sciences, under Contract W-31-109-Eng-38. Data were collected at Southeast Regional Collaborative Access Team (SER-CAT) beamlines at the Advanced Photon Source, Argonne National Laboratory. A list of supporting member institutions may be found on the SER-CAT website.

REFERENCES

1. Zetola, N., Francis, J. S., Nuermberger, E. L., and Bishai, W. R. (2005) *Lancet Infect. Dis.* **5,** 275–286
2. Tenover, F. C., Biddle, J. W., and Lancaster, M. V. (2001) *Emerging Infect. Dis.* **7,** 327–332
3. Lowy, F. D. (1998) *N. Engl. J. Med.* **339,** 520–532
4. Eisenreich, W., Bacher, A., Arigoni, D., and Rohdich, F. (2004) *Cell. Mol. Life Sci.* **61,** 1401–1426
5. Wilding, E. I., Brown, J. R., Bryant, A. P., Chalker, A. F., Holmes, D. J., Ingraham, K. A., Iordanescu, S., So, C. Y., Rosenberg, M., and Gwynn, M. N. (2000) *J. Bacteriol.* **182,** 4319–4327
6. Bloch, K., Chaykin, S., Phillips, A. H., and De Waard, A. (1959) *J. Biol. Chem.* **234,** 2595–2604
7. Krepkiy, D., and Miziorko, H. M. (2004) *Protein Sci.* **13,** 1875–1881
8. Alvear, M., Jabalquinto, A. M., Eyzaguirre, J., and Cardemil, E. (1982) *Biochemistry* **21,** 4646–4650
9. Michihara, A., Sawamura, M., Nara, Y., Ikeda, K., and Yamori, Y. (1997) *J. Biochem.* **122,** 647–654
10. Chiew, Y. E., O'Sullivan, W. J., and Lee, C. S. (1987) *Biochim. Biophys. Acta* **916,** 271–278
11. Voynova, N. E., Fu, Z., Battaile, K. P., Herdendorf, T. J., Kim, J. J., and Miziorko, H. M. (2008) *Arch. Biochem. Biophys.* **480,** 58–67
12. Bonanno, J. B., Edo, C., Eswar, N., Pieper, U., Romanowski, M. J., Ilyin, V., Gerchman, S. E., Kycia, H., Studier, F. W., Sali, A., and Burley, S. K. (2001) *Proc. Natl. Acad. Sci. U.S.A.* **98,** 12896–12901
13. Byres, E., Alphey, M. S., Smith, T. K., and Hunter, W. N. (2007) *J. Mol. Biol.* **371,** 540–553
14. Geisbrecht, B. V., Bouyain, S., and Pop, M. (2006) *Protein Expr. Purif.* **46,** 23–32
15. Brøns-Poulsen, J., Nøhr, J., and Larsen, L. K. (2002) *Methods Mol. Biol.* **182,** 71–76
16. Reardon, J. E., and Abeles, R. H. (1987) *Biochemistry* **26,** 4717–4722
17. Cho, Y. K., Ríos, S. E., Kim, J. J., and Miziorko, H. M. (2001) *J. Biol. Chem.* **276,** 12573–12578
18. Vlattas, I., Dellureficio, J., Ku, E., Bohacek, R., and Zhang, X. (1996) *Bioorg. Med. Chem. Lett.* **6,** 2091–2096
19. Krepkiy, D. V., and Miziorko, H. M. (2005) *Biochemistry* **44,** 2671–2677
20. Otwinowski, Z., and Minor, W. (1997) *Methods Enzymol.* **276,** 307–326
21. McCoy, A. J., Grosse-Kunstleve, R. W., Storoni, L. C., and Read, R. J. (2005) *Acta Crystallogr. D Biol. Crystallogr.* **61,** 458–464
22. Arnold, K., Bordoli, L., Kopp, J., and Schwede, T. (2006) *Bioinformatics* **22,** 195–201
23. Kiefer, F., Arnold, K., Künzli, M., Bordoli, L., and Schwede, T. (2009) *Nucleic Acids Res.* **37,** D387–D392
24. Adams, P. D., Grosse-Kunstleve, R. W., Hung, L. W., Ioerger, T. R., McCoy, A. J., Moriarty, N. W., Read, R. J., Sacchettini, J. C., Sauter, N. K., and Terwilliger, T. C. (2002) *Acta Crystallogr. D Biol. Crystallogr.* **58,** 1948–1954
25. Emsley, P., and Cowtan, K. (2004) *Acta Crystallogr. D Biol. Crystallogr.* **60,** 2126–2132
26. Emsley, P., Lohkamp, B., Scott, W. G., and Cowtan, K. (2010) *Acta Crystallogr. D Biol. Crystallogr.* **66,** 486–501
27. Schüttelkopf, A. W., and van Aalten, D. M. (2004) *Acta Crystallogr. D Biol. Crystallogr.* **60,** 1355–1363
28. Thompson, J. D., Higgins, D. G., and Gibson, T. J. (1994) *Nucleic Acids Res.* **22,** 4673–4680
29. Gouet, P., Courcelle, E., Stuart, D. I., and Métoz, F. (1999) *Bioinformatics* **15,** 305–308
30. Zemla, A. (2003) *Nucleic Acids Res.* **31,** 3370–3374
31. Bernstein, F. C., Koetzle, T. F., Williams, G. J., Meyer, E. F., Jr., Brice, M. D., Rodgers, J. R., Kennard, O., Shimanouchi, T., and Tasumi, M. (1977) *Eur. J. Biochem.* **80,** 319–324
32. DeLano, W. L. (2002) *The PyMOL Molecular Graphics System,* DeLano Scientific LLC, San Carlos, CA
33. Rocchia, W., Alexov, E., and Honig, B. (2001) *J. Phys. Chem. B* **105,** 6507–6514
34. Rocchia, W., Sridharan, S., Nicholls, A., Alexov, E., Chiabrera, A., and Honig, B. (2002) *J. Comput. Chem.* **23,** 128–137
35. Glaser, F., Pupko, T., Paz, I., Bell, R. E., Bechor-Shental, D., Martz, E., and Ben-Tal, N. (2003) *Bioinformatics* **19,** 163–164
36. Altschul, S. F., Madden, T. L., Schäffer, A. A., Zhang, J., Zhang, Z., Miller, W., and Lipman, D. J. (1997) *Nucleic Acids Res.* **25,** 3389–3402
37. Fu, Z., Wang, M., Potter, D., Miziorko, H. M., and Kim, J. J. (2002) *J. Biol. Chem.* **277,** 18134–18142
38. Krissinel, E., and Henrick, K. (2007) *J. Mol. Biol.* **372,** 774–797
39. Nave, J. F., d'Orchymont, H., Ducep, J. B., Piriou, F., and Jung, M. J. (1985) *Biochem. J.* **227,** 247–254
40. Fan, C., Fromm, H. J., and Bobik, T. A. (2009) *J. Biol. Chem.* **284,** 20240–20248
41. Ballard, F. J. (1966) *Biochem. J.* **101,** 70–75
42. Beytia, E., Dorsey, J. K., Marr, J., Cleland, W. W., and Porter, J. W. (1970) *J. Biol. Chem.* **245,** 5450–5458
43. Jabalquinto, A. M., and Cardemil, E. (1989) *Biochim. Biophys. Acta* **996,** 257–259
44. Gulbinsky, J. S., and Cleland, W. W. (1968) *Biochemistry* **7,** 566–575
45. Pilloff, D., Dabovic, K., Romanowski, M. J., Bonanno, J. B., Doherty, M., Burley, S. K., and Leyh, T. S. (2003) *J. Biol. Chem.* **278,** 4510–4515
46. Fromm, H. J. (1979) *Methods Enzymol.* **63,** 467–486
47. Krishna, S. S., Zhou, T., Daugherty, M., Osterman, A., and Zhang, H. (2001) *Biochemistry* **40,** 10810–10818
48. Timson, D. J., and Reece, R. J. (2002) *Biochimie* **84,** 265–272
49. Hartley, A., Glynn, S. E., Barynin, V., Baker, P. J., Sedelnikova, S. E., Verhees, C., de Geus, D., van der Oost, J., Timson, D. J., Reece, R. J., and Rice, D. W. (2004) *J. Mol. Biol.* **337,** 387–398
50. Hellinga, H. W., and Evans, P. R. (1987) *Nature* **327,** 437–439

Supplementary Material

CRYSTAL STRUCTURES OF *STAPHYLOCOCCUS EPIDERMIDIS* MEVALONATE DIPHOSPHATE DECARBOXYLASE BOUND TO INHIBITORY ANALOGS REVEAL NEW INSIGHT INTO SUBSTRATE BINDING AND CATALYSIS*

Michael L. Barta[‡,1], D. Andrew Skaff[§,1], William J. McWhorter[‡], Timothy J. Herdendorf[§], Henry M. Miziorko[§,2], and Brian V. Geisbrecht[‡,2]

From Division of Cell Biology and Biophysics[‡], Molecular Biology and Biochemistry[§], School of Biological Sciences, University of Missouri-Kansas City; Kansas City, Missouri 64110

Running Head: Inhibitor–mevalonate diphosphate decarboxylase structures

SUPPLEMENTARY FIGURE LEGENDS

Fig. S1. **Complete structure-based multiple sequence alignment of MDD proteins.** Alignment was generated using ClustalW. Numbers above the sequences correspond to *S. epidermidis* MDD. Red stars below the sequences correspond to invariant amino acid side chains involved in DPGP and FMVAPP interaction, while the green star represents the single variable active site residue.

Fig. S2. **Analytical size-exclusion chromatography of recombinant *S. epidermidis* MDD.** *A*, Purified MDD was injected onto a Tricorn 10/300 Superdex 200 (GE Bioscience) analytical size-exclusion chromatography column and its retention time was compared to a series of globular protein standards (BioRad). *B*, Size-exclusion calibration curve for four globular protein standards. The apparent molecular weight (*M.W.*) for MDD was estimated from observed elution volume (*E.V.*) using the equation: $M.W. = 29{,}649e^{-0.431 \times E.V.}$. For an elution volume of 14.05 ml, this yields an apparent molecular weight of 64 kDa.

SUPPLEMENTARY TABLES

Tables S1 and S2. **Intermolecular contacts between *S. epidermidis* MDD and the inhibitors DPGP and FMVAPP.** Distances for polar contacts between selected atoms of the MDD protein and inhibitors DPGP (Table S1) and FMVAPP (Table S2). In Table S2, distances are shown for both the wild-type and $Ser^{192} \rightarrow Ala$ forms of MDD bound to FMVAPP.

FIG. S1

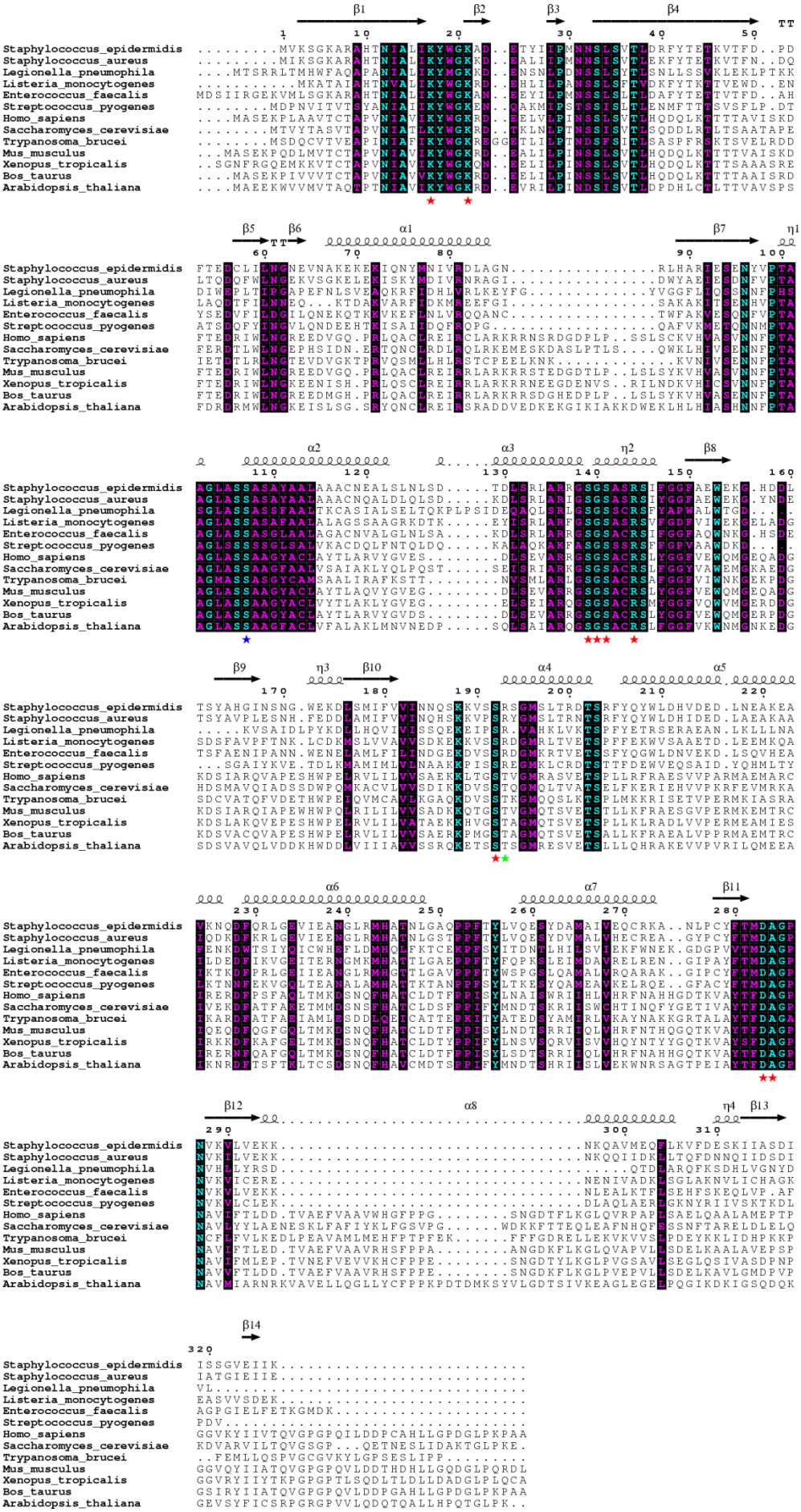
Staphylococcus_epidermidis
Staphylococcus_aureus
Legionella_pneumophila
Listeria_monocytogenes
Enterococcus_faecalis
Streptococcus_pyogenes
Homo_sapiens
Saccharomyces_cerevisiae
Trypanosoma_brucei
Mus_musculus
Xenopus_tropicalis
Bos_taurus
Arabidopsis_thaliana

FIG. S2

A

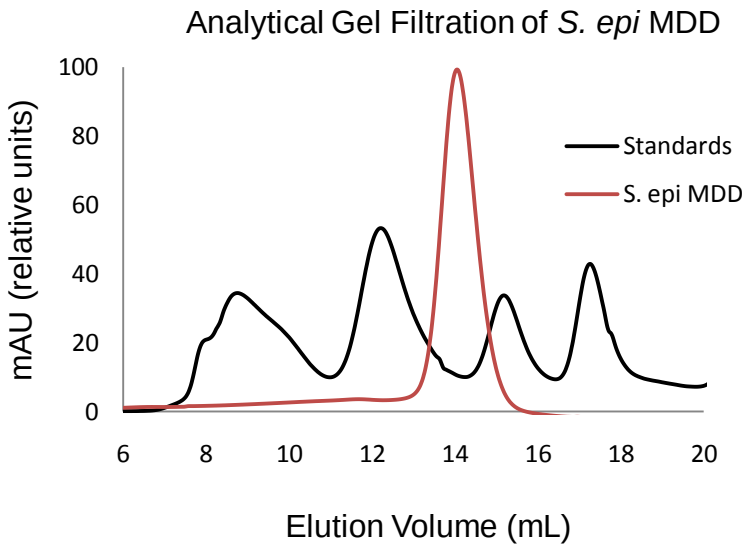
Analytical Gel Filtration of S. epi MDD
mAU (relative units)
100
80
60
40
20
0
6
8
10
12
14
16
18
20
Elution Volume (mL)
Standards
S. epi MDD

B

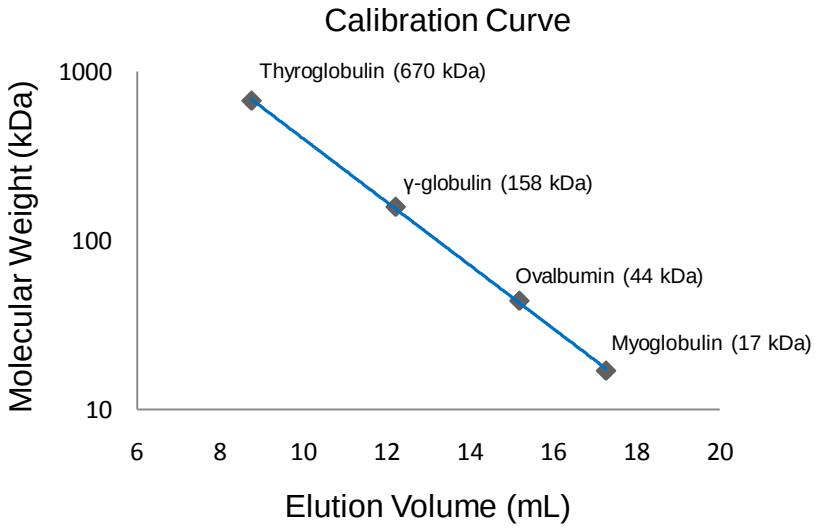
Calibration Curve
Molecular Weight (kDa)
1000
100
10
Thyroglobulin (670 kDa)
γ-globulin (158 kDa)
Ovalbumin (44 kDa)
Myoglobulin (17 kDa)
6
8
10
12
14
16
18
20
Elution Volume (mL)

Supplemental Tables 1 & 2

Table S1. MDD + DPGP Contacts

Enzyme		Distance (Å)	Inhibitor	
Amino Acid	Atom	DPGP	Atom	Group
Tyr18	OH	2.7	OAF	β-phosphoryl
Lys21	NZ	2.6	OAC	β-phosphoryl
Ser107	OG	2.9	OAD	α-phosphoryl
Ser139	OG	3.1	OAH	α-phosphoryl
Ser139	OG	3.1	OAG	β-phosphoryl
Gly140	N	2.9	OAF	β-phosphoryl
Ser141	OG	2.6	OAH	α-phosphoryl
Ser141	N	3.1	OAD	α-phosphoryl
Arg144	NH2	2.8	O	Carboxylate
Arg144	NH1	3.1	O	Carboxylate
Ser192	OG	3.0	OAM	α-phosphoryl
Ser192	OG	3.2	OAB	C2-hydroxyl
Arg193	NH2	2.9	OAG	β-phosphoryl
Arg193	NE	2.8	OAC	β-phosphoryl

Table S2. MDD + FMVAPP Contacts

Enzyme		Distance (Å)		Inhibitor	
Amino Acid	Atom	FMVAPP	$Ser^{192}\rightarrow Ala$	Atom	Group
Tyr18	OH	2.8	2.7	OAF	β-phosphoryl
Tyr18	N	2.9	2.8	OAD	Carboxylate
Lys21	NZ	2.8	2.7	OAB	β-phosphoryl
Ser139	OG	3.2	3.0	OAC	α-phosphoryl
Ser139	OG	2.6	2.7	OAG	β-phosphoryl
Gly140	N	2.8	2.8	OAF	β-phosphoryl
Ser141	OG	2.8	2.7	OAC	α-phosphoryl
Ser141	N	3.0	3.0	OAC	α-phosphoryl
Arg144	NH2	2.9	3.0	OAA	Carboxylate
Arg144	NH1	3.1	3.1	OAD	Carboxylate
Ser192	OG	2.8	N/A	OAH	α-phosphoryl
Arg193	NH2	3.1	3.0	OAG	β-phosphoryl
Arg193	NE	2.7	2.7	OAB	β-phosphoryl
Asp283	OD	3.4	3.6	OAE	C3-hydroxyl
Ala284	N	3.1	3.1	FAI	Fluoromethyl

Crystal Structures of *Staphylococcus epidermidis* Mevalonate Diphosphate Decarboxylase Bound to Inhibitory Analogs Reveal New Insight into Substrate Binding and Catalysis

Michael L. Barta, D. Andrew Skaff, William J. McWhorter, Timothy J. Herdendorf, Henry M. Miziorko and Brian V. Geisbrecht

J. Biol. Chem. 2011, 286:23900-23910.
doi: 10.1074/jbc.M111.242016 originally published online May 11, 2011
